SOLAR CELLS

Light-induced lattice expansion leads to high-efficiency perovskite solar cells

Hsinhan Tsai,[1,2] Reza Asadpour,[3] Jean-Christophe Blancon,[1] Constantinos C. Stoumpos,[4] Olivier Durand,[5] Joseph W. Strzalka,[6] Bo Chen,[7] Rafael Verduzco,[2,8] Pulickel M. Ajayan,[2] Sergei Tretiak,[9] Jacky Even,[5] Muhammad Ashraf Alam,[3] Mercouri G. Kanatzidis,[4] Wanyi Nie,[1]* Aditya D. Mohite[1,8]*

Light-induced structural dynamics plays a vital role in the physical properties, device performance, and stability of hybrid perovskite–based optoelectronic devices. We report that continuous light illumination leads to a uniform lattice expansion in hybrid perovskite thin films, which is critical for obtaining high-efficiency photovoltaic devices. Correlated, in situ structural and device characterizations reveal that light-induced lattice expansion benefits the performances of a mixed-cation pure-halide planar device, boosting the power conversion efficiency from 18.5 to 20.5%. The lattice expansion leads to the relaxation of local lattice strain, which lowers the energetic barriers at the perovskite-contact interfaces, thus improving the open circuit voltage and fill factor. The light-induced lattice expansion did not compromise the stability of these high-efficiency photovoltaic devices under continuous operation at full-spectrum 1-sun (100 milliwatts per square centimeter) illumination for more than 1500 hours.

Recent breakthroughs in the power conversion efficiency (PCE) of hybrid perovskites have been achieved by compositional engineering of the ABX_3 structure, where A and B are cations and X is an anion, in mixed-cation mixed-halide perovskites. This approach allows the formation of a stable cubic phase with suppressed nonradiative recombination for exceptionally high open-circuit voltage (V_{OC}) and short-circuit current density (J_{SC}) (*1*–*5*). Similar strategies were also applied by Snaith and coworkers to achieve a near-ideal band-gap material to create perovskite-perovskite tandem cells (*6*). Nonetheless, several recent reports (*7*–*11*) have led to the realization that dynamic light-induced structural changes play a vital role in the observed optoelectronic properties, performances, and long-term stability of devices. Charge-carrier recombination can be altered by constant illumination, which was proposed to be closely linked with ionic movement, defect passivation, or local polarization triggered by light (*12*–*15*). Local cation rotation or structural dynamics under light exposure can affect photophysical and electronic properties of methylammonium lead triiodide ($MAPbI_3$) (*16*–*18*). Wu and co-workers used ultrafast electron diffraction on $MAPbI_3$ thin films under illumination to experimentally elucidate the relationship between light-induced methylammonium (MA) rotation and the dynamics of hot carriers (*19*). Also, Zhou *et al.* indirectly attributed the post-illumination changes in the lattice to the weakening of the hydrogen bonding between MA and iodide (*20*).

Although these studies illustrate the importance of understanding these changes in the structure under light soaking, a direct and correlated in situ study monitoring the crystal structure transformations and their implications for photovoltaic (PV) performance, without invoking ionic migration, is still lacking. Such a study is also critical for understanding the microscopic origin of several reported light-induced changes in devices, such as ion migration near the interfaces, local polarization effects, and photoinduced degradation (*21*–*25*). Areas in need of research include mixed-cation halide perovskites, which offer the potential to approach the thermodynamic limit for a single-junction PV device with technologically relevant stability.

We report that continuous light soaking using a standard 1-sun (100 mW/cm^2) source causes a large and uniform lattice expansion. In a stabilized mixed-cation pure-iodide system, the light-induced lattice expansion resulted in an increase in the average structural correlation length and relaxation of the local strain. Comprehensive device characterization coupled with quantitative device modeling suggests that lattice expansion leads to two effects that improve the PCE: namely, reduction in the energetic barrier near the perovskite-contact interface and reduction in the nonradiative recombination, both in the bulk and in the interface. We observed a substantial improvement, from 18.5 to 20.5%, in the average PCE of a planar solar cell with a structure of fluorine-doped tin oxide–lithium-doped nickel oxide–formamidinium $(FA)_{0.7}MA_{0.25}Cs_{0.05}PbI_3$–fullerene–aluminum, with stability exceeding 1500 hours.

The $FA_{0.7}MA_{0.25}Cs_{0.05}PbI_3$ perovskite thin films were fabricated by mixing the precursors at desired stoichiometric ratios and spin-coated by our recently developed hot-casting method (*26*, *27*) (see the methods section in the supplementary materials). Figure 1A shows the synchrotron grazing-incidence wide-angle x-ray scattering (GIWAXS) map (left panel) for the $FA_{0.7}MA_{0.25}Cs_{0.05}PbI_3$ perovskite and the line cut (right panel) taken from the GIWAXS map. The peaks were indexed based on the cubic phase of $MAPbI_3$ perovskites with larger lattice constants, indicating that FA was incorporated within the lattice forming the cubic structure (the supplementary text and fig. S1 provide detailed analysis of GIWAXS for various compositions). Moreover, the addition of 5% Cs stabilized the cubic phase, which otherwise undergoes phase segregation (fig. S2), at room temperature (*6*, *28*). The band gap shifted from 1.66 eV for the $MAPbI_3$ thin film to 1.56 eV for the mixed-cation pure-iodide thin film (fig. S3), reflecting the incorporation of FA (*28*, *29*).

To examine the structural transformation of the $FA_{0.7}MA_{0.25}Cs_{0.05}PbI_3$ thin films under constant illumination, we used in situ GIWAXS measurement under intermediate vacuum pressure (10^{-5} torr) at 25°C ± 0.5°C with a controlled cooling stage (Fig. 1, A to E). Figure 1A (right panel) shows the line cuts obtained from in situ GIWAXS maps of thin films with increasing illumination times from 0 to 180 min measured at 10-min intervals. No splitting or new Bragg peaks emerged after 180 min of continuous illumination, implying the absence of phase segregation or degradation under continuous 1-sun illumination. However, all of the diffraction peaks uniformly shifted toward lower values of scattering vector **q**, corresponding to an isotropic increase in lattice constant *d* (lattice expansion) from 6.290 ± 0.002 Å to 6.330 ± 0.004 Å (Fig. 1B). This 1.4% change in the $FA_{0.7}MA_{0.25}Cs_{0.05}PbI_3$ thin film was the same as the expansion seen in a complete PV device with contact layers (fig. S4). We also observed a similar response for pure $MAPbI_3$ thin films, which suggests that light-induced lattice expansion is a general property of hybrid perovskites (fig. S5).

Even after the films rested in the dark, the lattice expansion persisted for 30 min before the lattice relaxed back to its original, pre–light exposure value (dashed lines in Fig. 1, A and C). We could exclude heat-induced lattice expansion because *d* remained unchanged after films were heated to 50°C (fig. S6). We also observed an increase in main-peak intensities associated with sharpening of the peak widths after illumination (Fig. 1C), suggesting improved crystallinity. Indeed, the full width at half maximum (FWHM) of the peak as a function of illumination time (Fig. 1D)

[1]Division of Materials Physics and Application, Los Alamos National Laboratory (LANL), Los Alamos, NM 87545, USA. [2]Department of Materials Science and NanoEngineering, Rice University, Houston, TX 77005, USA. [3]School of Electrical and Computer Engineering, Purdue University, West Lafayette, IN 47907, USA. [4]Department of Chemistry and Department of Materials Science and Engineering, Northwestern University, Evanston, IL 60208, USA. [5]Université de Rennes, Institut National des Sciences Appliquées (INSA) de Rennes, CNRS, Institut FOTON (Fonctions Optiques pour les Technologies de l'Information)—UMR 6082, F-35000 Rennes, France. [6]Division of X-Ray Science, Argonne National Laboratory, Argonne, IL 60439, USA. [7]Smalley-Curl Institute, Rice University, Houston, TX 77005, USA. [8]Department of Chemical and Biomolecular Engineering, Rice University, Houston, TX 77005, USA. [9]Division of Theoretical Chemistry and Molecular Physics, LANL, Los Alamos, New Mexico 87545, USA.
*Corresponding author. Email: wanyi@lanl.gov (W.N.); amohite@lanl.gov (A.D.M.)

decreased rapidly in the first 20 min and then more slowly during the next 2 hours. To evaluate the crystallite size (the coherent domain size of diffraction) and strain distribution, we performed a detailed structural analysis using a line profile (integral breadths) analysis of all of the diffraction planes on the basis of the Halder-Wagner equation (see the methods section in the supplementary materials and Fig. 1E). The coherence length, which describes the average crystallite size, was obtained from the slope of the linear fit of the Halder-Wagner plot. After light soaking, we observed a reduction in the y intercepts and thus a decrease in the microstrains, along with a reduction in the slope that resulted from an increase in the average crystallite size. The decrease in microstrains along with the increase in the crystallite size after illumination is indicative of the relaxation of the local strain in hybrid perovskites containing multiple cations. We propose a possible microscopic origin for the lattice expansion (Fig. 1F) as follows: The as-prepared thin film is strained because of the distorted nature of the lattice, which balances cations of different sizes. Upon illumination, it undergoes volumetric expansion in all directions. This process relaxes the local strain, reducing the mosaicity of the crystallites and sharpening the Bragg peaks.

We rationalize that on the microscopic scale, illuminating the hybrid perovskite films with photon energies greater than the band gap develops electron-hole pairs in the material. The photogenerated electrons in the conduction band can populate bonding states, whereas holes in the valence band vacate antibonding states. Both processes can weaken covalent bonds and lead to either less-distorted Pb–I–Pb bonds or elongation of the Pb–I bonds, which causes lattice expansion. From the photoluminescence (PL) measurements of the mixed-cation perovskite thin films before and after illumination, the emission peak undergoes a 5-meV red shift (fig. S10), which has been proposed for an enlarged unit cell caused by the increase of the Pb–I–Pb bond angle (*30*), whereas for Pb–I bond elongation, a blue shift should be expected (*31*). The lattice expansion observed did not originate exclusively from light-induced ion migration effects reported previously (*21*–*23*, *32*). In fact, x-ray photoelectron spectroscopy (XPS) with depth profiling of mixed-cation thin films performed before and after illumination showed the absence of an ion migration mechanism (figs. S7 and S8). More precisely, change in the I/Pb chemical ratio after light illumination, a signature of the redistribution of the halide (iodide) (*22*), was absent in the $FA_{0.7}MA_{0.25}Cs_{0.05}PbI_3$ mixed-cation system.

Realizing that the reduced mosaicity and improved crystallinity (Fig. 1) may lead to highly efficient and reliable solar cells, we fabricated a set of planar PV devices with nickel oxide and fullerene as selective contacts on the hole and electron collector sides, respectively (see the methods section in the supplementary materials). We directly analyzed the effect of light-induced lattice expansion on the device behavior by in situ monitoring of the structure (through GIWAXS) and PV figures of merit. We extracted the figures of merit from the current density–voltage (J-V) curve as a function of illumination time (Fig. 2A) and compared the change in those values with the change in the lattice constant (Fig. 2B). Figure 2A shows the time evolution of the V_{OC}, the fill factor (FF), and the J_{SC}. We observed an increase in the V_{OC} (Fig. 2A, top) from 0.73 to 0.9 V in the first 20 min, and then the V_{OC} gradually increased to 1.08 V during the next 120 min. The FF increased steadily from 60 to 74% with 2 hours of illumination, and the J_{SC} remained relatively unchanged.

Correlating the changes in device parameters ($\Delta V/V_0$ and $\Delta FF/FF_0$, where ΔV and ΔFF are the change in V and the change in FF, respectively, and V_0 and FF_0 are the initial values before illumination) (Fig. 2A) with the lattice constant difference ($\Delta d/d$) obtained from GIWAXS mapping (Fig. 1, A and B) as a function of illumination time (Fig. 2B) showed that the increase in the V_{OC} and FF and the increase in the lattice constant were synchronized. After 120 min of light soaking, both the lattice expansion and the V_{OC} and FF levels were saturated. Figure 2C illustrates the typical dark (dashed lines) and light (solid lines) J-V curves measured before (blue) and after (red) 120 min of light soaking. The peak efficiency occurred after 2 hours of illumination, when the V_{OC} and FF reached their peak values. The efficiency of our best device, with 0.35 cm^2 of active area, was 20.5%, with a V_{OC} of 1.08 V, a J_{SC} of 24.35 mA/cm^2, and an FF of 76.6%, and the statistical average efficiency (over 30 devices) was 19.35% with negligible hysteresis (figs. S12 and S13). Figure 2D shows the corresponding external quantum efficiency (EQE) of a typical light-soaked device accompanied by an electroluminescence (EL) spectrum before and after light soaking. The EL spectrum showed a 10-meV red shift after light soaking. The red shift in the EL spectrum is twice that for PL (5 meV) after light soaking, implying that the influence of lattice expansion may be more magnified in a device configuration where the perovskite is interfaced with rigid contact materials.

To understand the correlated improvement in the V_{OC} and FF caused by light-induced lattice expansion, we conducted measurements in both thin-film and device structures. The PL intensity

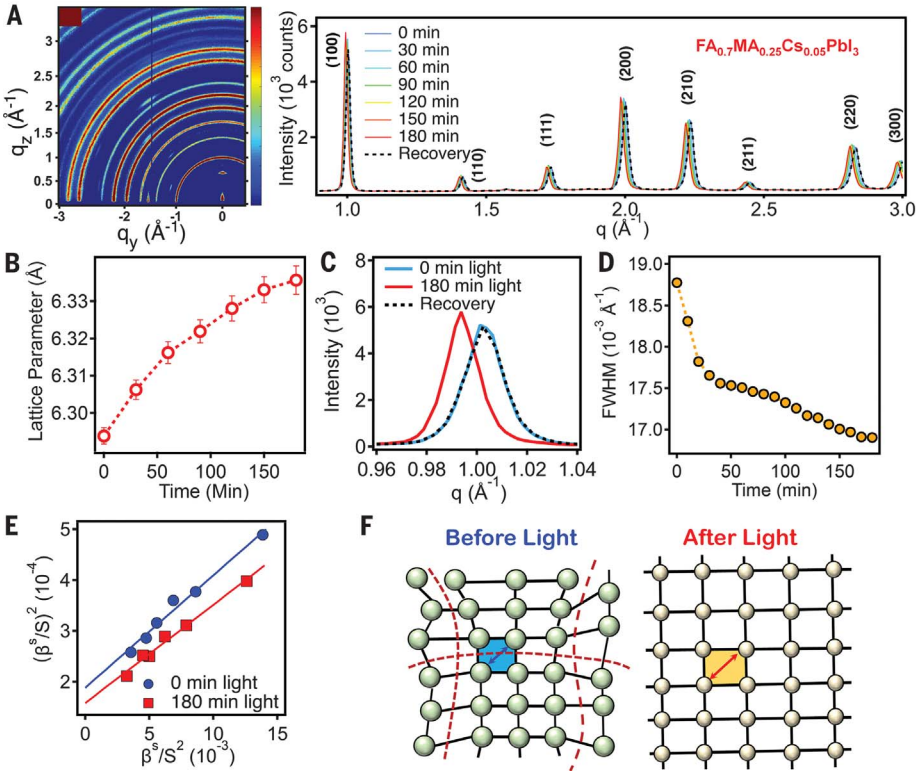

Fig. 1. Light-induced lattice expansion and structural analyses. (**A**) A typical synchrotron diffraction pattern (left) and the line cut of GIWAXS maps (right) for $FA_{0.7}MA_{0.25}Cs_{0.05}PbI_3$ (cubic phase) thin films under various illumination times and the recovery spectra obtained after the films were kept in the dark for 30 min. q_y, vector along in-plane direction, and q_z, vector along out-of-plane direction in reciprocal space with respect to the substrate. (**B**) Lattice constant as a function of illumination time. Error bars indicate the error from peak fitting. (**C**) Peak change before and after 180 min of illumination and recovery in the dark. (**D**) Full width at half maximum (FWHM) for peak as a function of illumination time. (**E**) Linear fit of integral-breadth analysis using Halder-Wagner plots, where β is the integral breadth of the diffraction peak and S is defined as $S = q/2\pi$. (**F**) Schematic describing the crystal structure change before illumination (local distortion) and after illumination (lattice expansion).

in the bulk film after light soaking increased by roughly a factor of 2 (fig. S10), suggesting passivation of trap states in the film. The PL intensity offers information on the radiative recombination efficiency in the thin film, which is correlated to the intrinsic quasi-Fermi level splitting without considering the contacts. However, such a small increase in the radiative efficiency corresponds to a gain of merely a few tens of millielectron volts in quasi-Fermi level splitting and does not account for the observed increase in V_{OC} of >200 mV after light soaking.

To understand the increase in the V_{OC}, we investigated the variations in the charge collection by performing a detailed analysis of the *J-V* curves coupled with a quantitative device model before and after illumination (Fig. 3, A and B; figs. S14 to S16; and tables S1 to S4). Examination of the slope of the *J-V* curves (obtained by taking the derivative of curves in Fig. 2C) as a function of applied voltage (Fig. 3A) revealed a slow rise near the low-field regime (0.5 to 0.7 V) before extended light soaking. The functional form converted to an S-shaped curve near the V_{OC}, indicative of field-dependent charge collection. Such behavior is also reflected in the crossover observed near the low-field regime in the dark and light *J-V* curves before light soaking (Fig. 2C). Both of these observations are signatures for the presence of an energetic barrier at the perovskite-contact interface in a p-i-n junction device (*33*, *34*).

Both the S-shaped curve and dark-light *J-V* crossing near the flat-band condition diminished after 2 hours of light soaking when lattice expansion occurred. We simulated the dark and light *J-V* curves and calculated the energy-band dispersion with a quantitative device model (Fig. 3B, red and blue solid lines). A good fit to the experimental *J-V* curves was obtained only by including a band misalignment (Fig. 3B) at the perovskite-contact interface for the device before light soaking (figs. S14 to S16). The band misalignment translates to a barrier for electrons injected from the electron-transporting material and holes injected from the hole-transporting material near the flat-band condition. The photogenerated carriers lose their energy through recombination, reducing the charge collection efficiency at low fields.

We experimentally confirmed the presence of such an energetic barrier before light soaking and its removal thereafter by directly probing the flat-band voltage ($V_{FLATBAND}$) of the PV device by measuring the amplitude of the electroabsorption (EA) signal at the band-edge energy (794 nm) as a function of applied direct current (DC) bias (V_{DC}) (Fig. 3C, the method section in the supplementary materials, and fig. S17) (*35*). Briefly, the EA signal amplitude vanished at the absorber band edge once the applied bias compensated for the internal electric field when the device reached the flat-band condition. We observed a 200-mV increase in $V_{FLATBAND}$ after illumination, a direct indication of the reduction of the barrier after long-term light soaking (or lattice expansion). This increase resulted in efficient charge collection in the low-field (0.5 to 0.9 V) regime. The substantial reduction of the interfacial barrier was also consistent with the measured EL EQE (EQE_{EL}) and the forward injection current (J_{INJ}) as a function of applied voltage before and after light soaking (Fig. 3D). The EQE_{EL} measured when the device was driven at low voltage increased by 100 times after extended illumination. We attribute this increase to the reduced nonradiative recombination current and improved EL intensity. Before illumination, both the hole and the electron injection were mitigated by the barrier, which would be more pronounced at one of the contacts (Fig. 3B and fig. S16). This difference resulted in a high recombination current at low voltage.

Our experimental results presented in Fig. 2 and 3 suggest that the effect of light-induced lattice expansion is directly reflected in PV operation through the improvement in the band alignment,

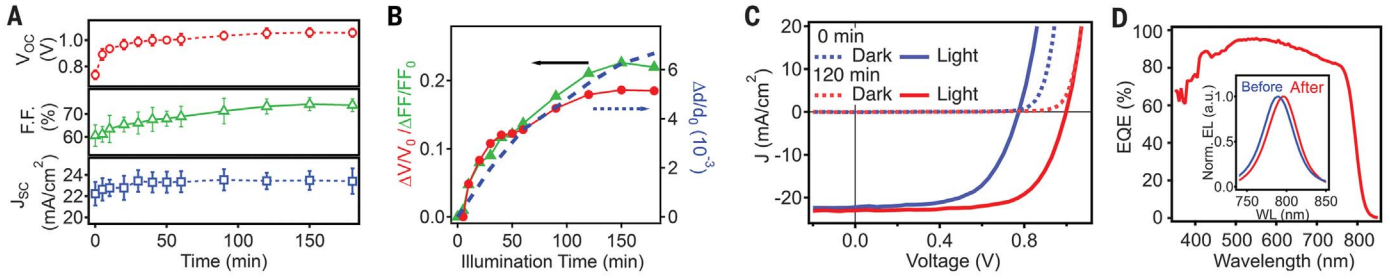

Fig. 2. Effect of light-induced lattice expansion on PV performance of $FA_{0.7}MA_{0.25}Cs_{0.05}PbI_3$ thin films. (**A**) Solar cell figures of merit as a function of illumination time. Error bars indicate statistical variation over 30 devices. (**B**) Changes in V_{OC} and FF ($\Delta V/V_0$ and $\Delta FF/FF_0$) correlated to the change in the lattice constant ($\Delta d/d_0$) as a function of light-soaking time, where V_0 and FF_0 are the initial points before illumination. (**C**) *J-V* curves obtained in the dark and under AM1.5G (global standard spectrum air mass) solar simulator illumination. (**D**) EQE for a typical device and the corresponding EL spectrum for the same device before and after 120 min of illumination. Norm., normalized; a.u., arbitrary units; WL, wavelength.

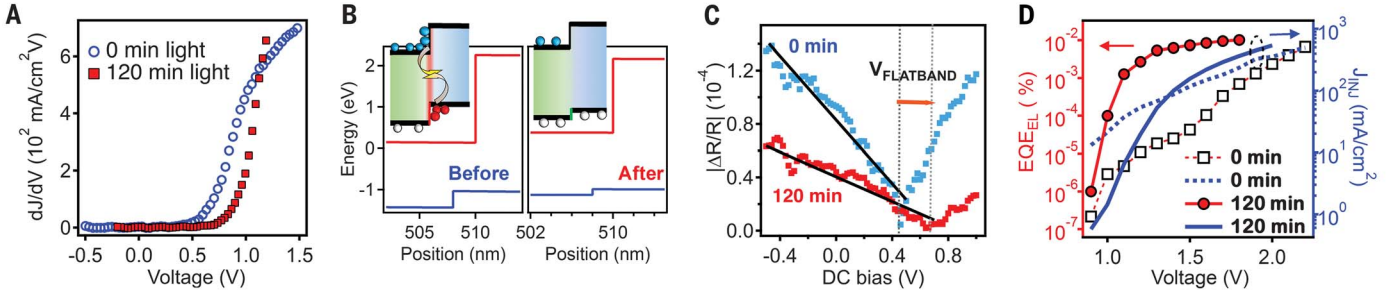

Fig. 3. Device and thin-film characteristics under constant illumination. (**A**) First-order derivative of the *J-V* curves (from Fig. 2C) before and after 2 hours of light soaking. (**B**) Calculated band alignment from the charge density profile based on the *J-V* fitting before and after light soaking, along with schematics illustrating the charge collection and recombination processes at the interface. (**C**) Device flat-band voltage ($V_{FLATBAND}$) before and after light soaking for 2 hours, obtained by measuring the EA magnitude change as a function of DC bias. ΔR/R, change in reflection (ΔR) normalized by the linear reflection. (**D**) EL characteristics for the same device before and after illumination, plotted as EQE_{EL} (left) and current density J_{INJ} (right) versus voltage.

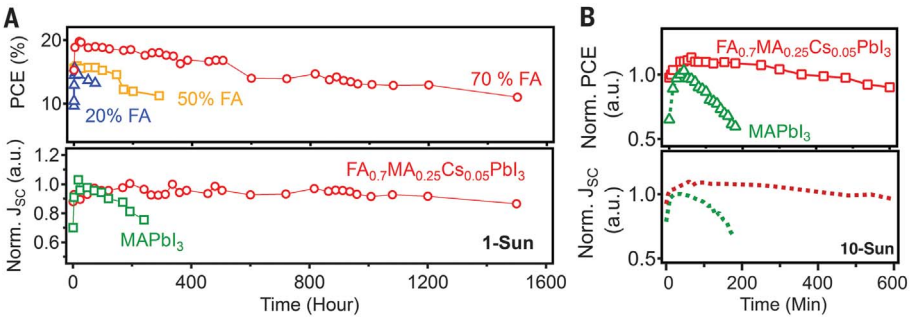

Fig. 4. Photostability studies. Long-term photostability test under constant 1-sun (**A**) and 10-sun (**B**) illumination, carried out by monitoring the time evolution of device PCE and J_{SC}.

which enhances the build-in voltage and suppresses the interfacial nonradiative recombination, as indicated by increases in the EL, the V_{OC}, and the FF. However, the J_{SC} remains largely unaffected because of the presence of a large internal field at short circuit, coupled with the long diffusion of mixed-cation perovskites (*4*, *6*). These results also suggest that the influences of light-induced lattice expansion and strain relaxation are most magnified at one of the interfaces and facilitate the suppression of the energetic barrier.

Interface modification after light soaking was previously observed in a $MAPbI_3$ system (*22*, *24*, *36*) and was attributed to the iodide migration toward the contact that effectively doped the interface. To exclude this possibility in our system, two experiments were designed: XPS depth profiling (experiment one) and a control experiment of applying a bias in the dark (experiment two). Experiment one directly probed the ion (Pb^{2+} and I^-) distribution before and after illumination. As no change in halide distribution occurred (fig. S7 and S8), we excluded halide redistribution in the mixed-cation system, a conclusion that is further supported by PL map measurements (figs. S10 and S11). In experiment two, we monitored V_{OC} and FF values for PV devices under constant bias in the dark to probe whether ion migration occurred under an applied electrical field. Given the data obtained (supplementary text and figs. S18 and S19), we did not observe any appreciable change in device performance after dark biasing with a constant current. These experimental results are direct proof of lack of ion migration in the system and unambiguously demonstrate that light-induced lattice expansion is the dominant mechanism responsible for lowering the interface barrier and improving the V_{OC} and FF. The lack of evidence for ion migration in the mixed cation is also consistent with some recent studies (*6*, *28*) in which no degradation was observed, suggesting that ion migration does not dominate the properties in these systems. However, our observed mechanism can be correlated to the recently suggested local ionic movements activated by light (*32*, *36*–*39*) and may provide insight into the structural origin for those observed phenomena. Moreover, lattice expansion–induced interfacial changes have also been observed in oxide perovskite interfaces (in $SrTiO_3$ and $BiFeO_3$), silicon–silicon dioxide interfaces (*40*), and other classical semiconductors. However, in contrast to most reports on superconductors [for example, (*41*)], our study describes a beneficial effect from the light-induced lattice expansion.

Finally, we verified that the light-induced lattice expansion was not detrimental to device stability. We assessed our PV device under a wide range of operating conditions and external stresses (Fig. 4 and fig. S18). Figure 4 shows the long-term stability of encapsulated devices obtained by monitoring the PCE and J_{SC} under 1- and 10-sun illuminations (see the methods section in the supplementary materials). The PCE retained 85% of the peak value after 800 hours of continuous operation at the maximum power point. The J_{SC} did not undergo any observable photoinduced degradation during more than 1500 hours of continuous illumination. The drop in PCE results from a loss in FF, which we believe is consistent with the degradation of the Al contact and is a result of the fullerene-Al interface (*3*).

We also performed aggressive stability tests under 10-sun solar intensities (Fig. 4B). In contrast to $MAPbI_3$-based devices, which degrade within 30 min, the $FA_{0.7}MA_{0.25}Cs_{0.05}PbI_3$ devices maintained 95% of their efficiency for 300 min and then degraded to 80% over 600 min. The J_{SC} (Fig. 4B, bottom) maintained 96% of the original value even after 600 min of 10-sun illumination. We performed further stability tests by increasing the current injection in EL, the J_{SC} as a function of light intensity, and the time-dependent EQE (fig. S21 and supplementary text), which further demonstrated the technologically relevant durability of mixed-cation pure-halide perovskites for low-cost, high-efficiency optoelectronic applications. We believe that our results demonstrating light-induced lattice expansion independent of ion migration will motivate the exploration of new behaviors and structural phases in hybrid perovskites, analogous to those observed in complex oxides under nonequilibrium conditions and external stimuli.

REFERENCES AND NOTES

1. W. S. Yang *et al.*, *Science* **356**, 1376–1379 (2017).
2. C. Yi *et al.*, *Energy Environ. Sci.* **9**, 656–662 (2016).
3. M. Saliba *et al.*, *Science* **354**, 206–209 (2016).
4. D. Bi *et al.*, *Sci. Adv.* **2**, e1501170 (2016).
5. N. J. Jeon *et al.*, *Nature* **517**, 476–480 (2015).
6. D. P. McMeekin *et al.*, *Science* **351**, 151–155 (2016).
7. S. Draguta *et al.*, *Nat. Commun.* **8**, 200 (2017).
8. K. Zheng *et al.*, *J. Phys. Chem. Lett.* **7**, 4535–4539 (2016).
9. M. Sendner *et al.*, *Mater. Horiz.* **3**, 613–620 (2016).
10. W. Nie *et al.*, *Nat. Commun.* **7**, 11574 (2016).
11. D. W. deQuilettes *et al.*, *Science* **348**, 683–686 (2015).
12. S. Chen *et al.*, *Sol. RRL* **1**, 1600001 (2017).
13. S. Shao *et al.*, *Adv. Funct. Mater.* **26**, 8094–8102 (2016).
14. S. Meloni *et al.*, *Nat. Commun.* **7**, 10334 (2016).
15. R. Gottesman *et al.*, *J. Phys. Chem. Lett.* **5**, 2662–2669 (2014).
16. M. Bokdam *et al.*, *Sci. Rep.* **6**, 28618 (2016).
17. A. M. A. Leguy *et al.*, *Nat. Commun.* **6**, 7124 (2015).
18. C. Eames *et al.*, *Nat. Commun.* **6**, 7497 (2015).
19. X. Wu *et al.*, *Sci. Adv.* **3**, e1602388 (2017).
20. Y. Zhou *et al.*, *Nat. Commun.* **7**, 11193 (2016).
21. I. Zarazua, J. Bisquert, G. Garcia-Belmonte, *J. Phys. Chem. Lett.* **7**, 525–528 (2016).
22. D. W. deQuilettes *et al.*, *Nat. Commun.* **7**, 11683 (2016).
23. C. Zhao *et al.*, *Adv. Energy Mater.* **5**, 1500279 (2015).
24. Y. Deng, Z. Xiao, J. Huang, *Adv. Energy Mater.* **5**, 1500721 (2015).
25. H.-W. Chen, N. Sakai, M. Ikegami, T. Miyasaka, *J. Phys. Chem. Lett.* **6**, 164–169 (2015).
26. H. Tsai *et al.*, *Nature* **536**, 312–316 (2016).
27. W. Nie *et al.*, *Science* **347**, 522–525 (2015).
28. M. Saliba *et al.*, *Energy Environ. Sci.* **9**, 1989–1997 (2016).
29. G. E. Eperon *et al.*, *Energy Environ. Sci.* **7**, 982–988 (2014).
30. C. C. Stoumpos, M. G. Kanatzidis, *Adv. Mater.* **28**, 5778–5793 (2016).
31. S. Boyer-Richard *et al.*, *J. Phys. Chem. Lett.* **7**, 3833–3840 (2016).
32. Y.-C. Zhao *et al.*, *Light Sci. Appl.* **6**, e16243 (2017).
33. R. V. K. Chavali *et al.*, *IEEE J. Photovolt.* **5**, 865–873 (2015).
34. J. E. Moore, S. Dongaonkar, R. V. K. Chavali, M. A. Alam, M. S. Lundstrom, *IEEE J. Photovolt.* **4**, 1138–1148 (2014).
35. I. H. Campbell *et al.*, *Polym. Adv. Technol.* **8**, 417–423 (1997).
36. P. Calado *et al.*, *Nat. Commun.* **7**, 13831 (2016).
37. S. Ravishankar *et al.*, *J. Phys. Chem. Lett.* **8**, 915–921 (2017).
38. S. Shao *et al.*, *Energy Environ. Sci.* **9**, 2444–2452 (2016).
39. E. Mosconi, D. Meggiolaro, H. J. Snaith, S. D. Stranks, F. De Angelis, *Energy Environ. Sci.* **9**, 3180–3187 (2016).
40. S. Nonomura *et al.*, *J. Non-Cryst. Solids* **266–269**, 474–480 (2000).
41. N. Poccia *et al.*, *Nat. Mater.* **10**, 733–736 (2011).

ACKNOWLEDGMENTS

Funding: The work at LANL was supported by the Laboratory Directed Research and Development (LDRD) Directed Research (DR) project. The XPS analyses were done in Shared Equipment Authority (SEA) and were supported by Rice University. The GIWAXS maps were done at sector 8-ID-E of the Advanced Photon Source, a U.S. Department of Energy (DOE) Office of Science User Facility operated for the DOE Office of Science by Argonne National Laboratory under contract DE-AC02-06CH11357. Work at Northwestern was supported by the U.S. Department of Energy, Office of Science (grant SC0012541, structure characterization). A.D.M. acknowledges support by Office of Energy Efficiency and Renewable Energy grant DE-FOA-0001647-1544 for this work. **Author contributions:** W.N., H.T., and A.D.M. conceived the idea, designed experiments, and co-wrote the manuscript. H.T. fabricated and characterized the thin films and devices and analyzed data under the supervision of W.N. and A.D.M. C.C.S. and M.G.K. performed crystallography analysis of the powder diffraction and calculated the molecular structures. J.-C.B. conducted the optical spectroscopy measurements on the thin film and analyzed the data. R.A. performed device modeling simulations and analyzed simulation data with M.A.A., who conceived and supervised the device modeling. J.W.S. helped with GIWAXS experiment setup, and O.D. analyzed the GIWAXS data. B.C., R.V., and P.M.A. helped with XPS experiments and analyses. S.T. and J.E. were involved in discussion. All authors have read the manuscript and agree to its contents. **Competing interests:** None declared. **Data and materials availability:** All data needed to evaluate the conclusions in the paper are present in the supplementary materials.

SUPPLEMENTARY MATERIALS

www.sciencemag.org/content/360/6384/67/suppl/DC1
Materials and Methods
Supplementary Text
Figs. S1 to S21
Tables S1 to S9
References (*42*–*75*)

4 September 2017; resubmitted 15 December 2017
Accepted 9 February 2018
10.1126/science.aap8671

Light-induced lattice expansion leads to high-efficiency perovskite solar cells

Hsinhan Tsai, Reza Asadpour, Jean-Christophe Blancon, Constantinos C. Stoumpos, Olivier Durand, Joseph W. Strzalka, Bo Chen, Rafael Verduzco, Pulickel M. Ajayan, Sergei Tretiak, Jacky Even, Muhammad Ashraf Alam, Mercouri G. Kanatzidis, Wanyi Nie and Aditya D. Mohite

Science **360** (6384), 67-70.
DOI: 10.1126/science.aap8671

Light relaxes hybrid perovskites

Ion migration in organic-inorganic perovskite solar cells limits device stability and performance. Tsai *et al.* found that a cesium-doped lead triiodide perovskite with mixed organic cations underwent a uniform lattice expansion after 180 min of exposure at 1 sun of illumination. This structural change reduced the energy barriers for charge carriers at the contacts of solar cells. The resulting increase in power conversion efficiency from 18.5 to 20.5% was maintained for more than 1500 hours of illumination.

Science, this issue p. 67